Editors' Suggestion

Tuning a Two-Impurity Kondo System by a Moiré Superstructure

Sergey Trishin,[1] Christian Lotze,[1] Friedemann Lohss,[1] Giada Franceschi,[1] Leonid I. Glazman,[2] Felix von Oppen,[3] and Katharina J. Franke[1]

[1]*Fachbereich Physik, Freie Universität Berlin, 14195 Berlin, Germany*

[2]*Department of Physics, Yale University, New Haven, Connecticut 06520, USA*

[3]*Dahlem Center for Complex Quantum Systems and Fachbereich Physik, Freie Universität Berlin, 14195 Berlin, Germany*

(Received 4 January 2023; accepted 7 April 2023; published 27 April 2023)

Two-impurity Kondo models are paradigmatic for correlated spin-fermion systems. Working with Mn atoms on Au(111) covered by a monolayer of MoS_2, we tune the interadatom exchange via the adatom distance and the adatom-substrate exchange via the location relative to a moiré structure of the substrate. Differential-conductance measurements on isolated adatoms exhibit Kondo peaks with heights depending on the adatom location relative to the moiré structure. Mn dimers spaced by a few atomic lattice sites exhibit split Kondo resonances. In contrast, adatoms in closely spaced dimers couple antiferromagnetically, resulting in a molecular-singlet ground state. Exciting the singlet-triplet transition by tunneling electrons, we find that the singlet-triplet splitting is surprisingly sensitive to the moiré structure. We interpret our results theoretically by relating the variations in the singlet-triplet splitting to the heights of the Kondo peaks of single adatoms, finding evidence for coupling of the adatom spin to multiple conduction electron channels.

DOI: 10.1103/PhysRevLett.130.176201

Exchange interactions between magnetic adatoms and itinerant electrons of a substrate can induce correlation effects. For strong exchange coupling, the adatom spin becomes Kondo screened [1,2]. For intermediate coupling, where the Kondo temperature is comparable to temperature or other competing couplings, the Kondo renormalizations remain in the perturbative domain [3]. When the exchange coupling is weak, competing couplings such as single-ion anisotropy can dominate, in which case Kondo screening can be neglected and spin excitations can be probed [4]. The panorama becomes yet broader when exchange coupling the adatom to a second magnetic atom in its vicinity. The nature of this coupling depends on the interatomic spacing. In close proximity, direct exchange tends to dominate, while larger separations favor substrate-mediated couplings such as the oscillatory Rudermann-Kittel-Kasuya-Yosida (RKKY) [5–7] and Dzyaloshinskii-Moriya [8,9] interactions. The resulting ground states may be ferromagnetic [10,11], antiferromagnetic [10,11], or noncollinear [12].

The competition between interadatom and adatom-substrate exchange leads to a rich phase diagram with multiple correlated ground states. Theoretically, the two-impurity Kondo problem has been treated extensively [13,14], and motivated numerous experiments [10,15–18]. The parameter space can be most directly explored by scanning-tunneling-microscopy (STM) experiments. Atom manipulation with the STM tip admits maneuvering the atoms into lattice sites at various distances and thus investigating different interatomic interaction strengths [19]. Tuning of the exchange coupling to the surface is somewhat less straightforward. An early approach used strain-induced changes in the band gap of a decoupling interlayer [20]. A more controlled strategy would exploit well-defined superstructures. Prime candidates to impose a spatially periodic modulation of the atom-substrate interaction strength are interlayers which form moiré structures with the underlying metal substrate [21–23]. Most notably, monolayers of MoS_2 on Au(111) have been successfully employed for tuning the exchange coupling of single magnetic Fe atoms from essentially uncoupled to strongly Kondo screened [23].

Here, we exploit the moiré pattern formed by monolayer-MoS_2 on Au(111) to tune the exchange coupling of Mn dimers with the substrate, thereby probing the competition between interatomic and atom-substrate exchange. We find that the direct exchange coupling between closely spaced Mn atoms leads to a singlet ground state and study the remarkably strong variations of the singlet-triplet splitting across the moiré pattern. We introduce a new experimental signature of multichannel Kondo coupling by exploiting a theoretical relation between the singlet-triplet excitation energy of the dimer and the Kondo renormalizations of individual adatoms and find evidence that the Mn adatoms are coupled to several conduction-electron channels.

We use the previously established moiré-patterned decoupling layer MoS_2 on Au(111) [23], grown by depositing Mo atoms and subsequent annealing to 800 K in H_2S gas at a pressure of $p = 10^{-5}$ mbar [24,25]. A moiré structure forms as a result of the lattice mismatch between adlayer and substrate, seen in the STM images as a modulation of the apparent height with a periodicity of ≈3.3 nm

[Fig. 1(a)] [24–26]. Deposition of Mn atoms at low temperatures (< 10 K) leads to isolated atoms observable as round protrusions with an apparent height of ≈300 pm. Some round protrusions with smaller apparent height are attributed to Mn atoms attached to defects and excluded from further analysis. We also find some oval protrusions. As discussed in more detail below, we attribute these to Mn dimers.

We start by characterizing individual Mn atoms. These exhibit a narrow zero-bias resonance in differential-conductance (dI/dV) spectra as shown for two examples in Fig. 1(b). At our experimental temperature of 1.1 K, the line shape is well reproduced by a temperature-broadened logarithmic peak. The peak splits in a magnetic field [Fig. 1(c)]. At 3 T, the Zeeman split amounts to 600 μV. This behavior is reminiscent of a weakly coupled Kondo impurity, with the experimental temperature larger than or of the order of the Kondo temperature [3]. Mn atoms at different positions with respect to the moiré lattice exhibit line shapes with small variations in intensity, but the same broadening [see Fig. 1(b) for two extremal cases]. The intensity modulations can be understood as modulations of $J\nu_0$, where J is the strength of the exchange coupling to the conduction electrons and ν_0 the density of states (DOS) at the Fermi level as discussed in more detail below. The observed variations are consistent with the DOS modulations due to the adatoms' position on the moiré structure [Fig. 1(d)].

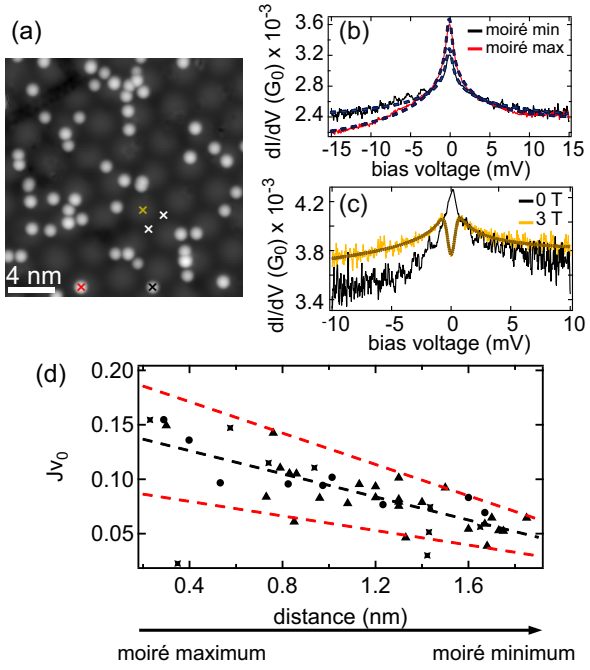

FIG. 1. Variation of the Kondo coupling across the moiré structure. (a) STM topography of Mn atoms on the moiré structure of MoS_2 on Au(111) (recorded at 100 mV, 20 pA). A moiré maximum (yellow), a hcp and fcc minimum (white) are indicated by crosses. (b) dI/dV spectra taken on Mn atoms adsorbed close to a moiré maximum (red) and a moiré minimum (black), locations indicated in (a). Dashed lines show fits using a code based on Ref. [27]. The fits yield a (dimensionless) adatom-substrate exchange $J\nu_0$ of −0.080 (red) and −0.049 (black). (c) dI/dV spectra on a Mn atom on a moiré minimum at 0 T (black) and 3 T (orange). The zero-bias resonance splits at 3 T (fit: dashed line). [Spectra recorded at a setpoint of 15 mV, 3 nA (b) and 10 mV, 3 nA (c)]. (d) Values of $J\nu_0$ obtained from fitting dI/dV spectra (keeping $T_0^2 = 0.000415$ constant, as obtained from a best fit with B field) on atoms at various positions within the moiré superstructure. Symbols indicate different measurement sets. The black dashed line is a linear guide to the eye through the data points. The red dashed lines are corresponding lines obtained from fits using different tunnel couplings T_0^2. The upper line corresponds to $T_0^2 = 2.635 \times 10^{-4}$ and the lower line to $T_0^2 = 5.6 \times 10^{-4}$. These boundary values have been determined from error margins of fits at 3 T.

Next, we characterize dimer structures formed by two adatoms in close proximity to each other. Density-functional calculations suggest that isolated atoms sit in hollow sites of the terminating S layer [28,29]. Starting with this assumption, we can tentatively assign model structures to the most commonly found dimer arrangements on the surface by evaluating the separation and orientation in the STM images. Figures 2(a) and 2(b) show an arrangement, where two Mn atoms are separated by three lattice sites of the MoS_2 substrate (for details of the structure analysis, see the Supplemental Material [30]). At this separation, the atoms show a Kondo resonance as previously described for individual adatoms [Fig. 2(c)], indicating that interatomic interactions are negligible. At a distance of two atomic lattice sites [Figs. 2(d) and 2(e)], the Kondo resonance develops a dip at the Fermi level [Fig. 2(f)]. The spectrum is reminiscent of a Zeeman-split Kondo resonance, indicating magnetic interactions between the atoms, presumably resulting from substrate-mediated RKKY interactions. When the atoms are in even closer proximity, their shapes are no longer individually resolved in the STM image [Figs. 2(g) and 2(h)]. While a definite assignment of the adsorption sites is thus difficult, the oval shape and its orientation with respect to the underlying lattice suggest that the atoms lie in nearest-neighbor hollow sites (for details, see the Supplemental Material [30]). Differential-conductance spectra measured on this type of dimer are radically different from those of individual atoms or weakly interacting dimers. The Kondo resonance is now replaced by pronounced inelastic steps at ±10 mV [Fig. 2(i)].

It is rather surprising to detect inelastic excitations of a relatively large energy, considering that individual atoms do not show a noticeable magnetocrystalline anisotropy. We suggest that the threshold energy is associated with a spin-changing transition of the dimer. Such excitations have been observed for Mn dimers on CuN [31]. The close proximity of the atoms may allow for direct exchange as a result of finite overlap of the atomic d orbitals. Mn atoms

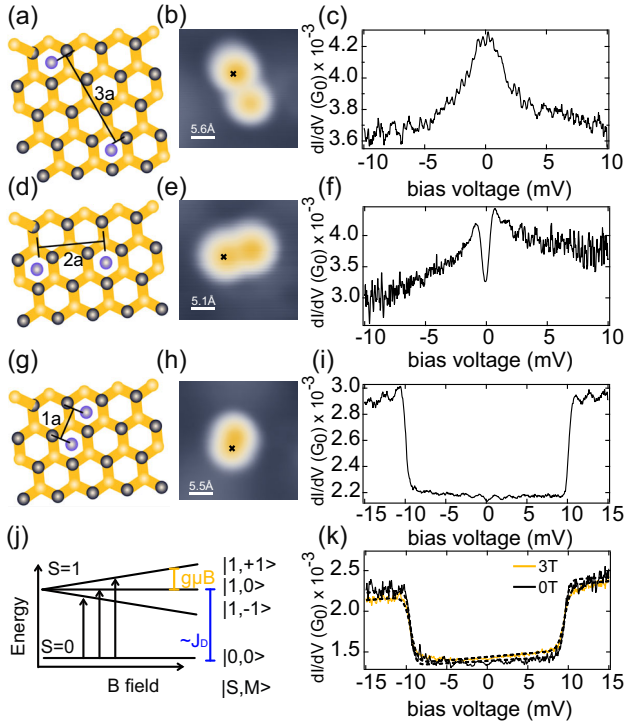

FIG. 2. Various dimer structures. (a),(d),(g) Structure models and (b),(e),(f) corresponding STM topographies of Mn dimers on MoS_2 with various interatom spacings. Yellow, gray, and purple spheres represent S, Mo, and Mn, respectively. The Mn atoms, sitting in MoS_2 hollow sites, are separated by three lattice sites (a),(b), two lattice sites (d),(e), and one lattice site (g),(h). (c),(f),(i) dI/dV spectra recorded at the locations indicated by black crosses in (b),(e),(h). The spectra drastically depend on the dimer separation, exhibiting a Kondo resonance (c), a split Kondo resonance (f), and a steplike increase in the differential conductance (i). (j) Energy-level diagram of the observed spin excitation in (i). The degeneracy of the $M = 0, \pm 1$ sublevels of the excited state is lifted by a magnetic field. (k) dI/dV spectra of a dimer with Mn in nearest-neighbor sites with and without magnetic field and respective fits with symmetric step functions (dashed). For our measurement conditions at 1.1 K, a magnetic field of 3 T is not sufficient to fully resolve the splitting, but the excitation appears broadened with a width of 0.29 ± 0.02 mV and 0.40 ± 0.01 mV at 0 and 3 T, respectively. STM topographies recorded at 100 mV, 20 pA, setpoint of the dI/dV spectra 10 mV, 3 nA (c), (f), 15 mV, 3 nA (i), and 20 mV, 3 nA (k).

are indeed likely coupled antiferromagnetically when interacting via direct exchange [32]. This would lead to a singlet ground state $|S_{\mathrm{tot}} = 0, M = 0\rangle$. Magnetic excitations must then involve a spin-changing transition such as the singlet-triplet transition, and the excitation energy directly reflects the exchange coupling J_D (for details, see below). To further corroborate the antiferromagnetic nature of the exchange coupling, we apply an external magnetic field of 3 T. The inelastic steps become slightly broader [Fig. 2(k)]. This is consistent with a singlet-triplet transition to $|S_{\mathrm{tot}} = 1, M\rangle$, where the excited state is Zeeman split in the magnetic field, but the sublevels are not individually resolved at the experimental temperature of 1.1 K [Fig. 2(j)]. Importantly, we do not observe additional excitations around zero bias, which would indicate a higher-spin ground state as favored by ferromagnetic coupling of the atoms.

As discussed above, the moiré superstructure weakly affects the height of the Kondo resonance of individual atoms reflecting the modulation of the dimensionless exchange coupling $J\nu_0$. As the dimer is in a singlet ground state, one may naively expect that the moiré structure does not influence the inelastic excitations. Remarkably, we observe strong variations of the singlet-triplet transition by several meV as the dimer's adsorption site is varied with respect to the moiré lattice (Fig. 3). Dimers located on maxima of the moiré structure [Figs. 3(a) and 3(e)] exhibit the smallest excitation energy (7.5 meV), while those on minima [Figs. 3(d) and 3(e)] show the largest excitation energy (10 meV). (We show an analysis of 39 dimers at different locations on the MoS_2 structure in the Supplemental Material [30]).

To understand these variations, we compute the shift of the singlet-triplet splitting Δ due to the hybridization of the adatom d orbitals with the substrate and relate it to the exchange coupling between the adatom and conduction-electron spins. As we do not observe inelastic excitations on single adatoms indicating negligible single-ion anisotropy, we assume that the Mn atoms are only weakly perturbed by the surrounding and retain the half-filled d shell when placed on the substrate. According to Hund's

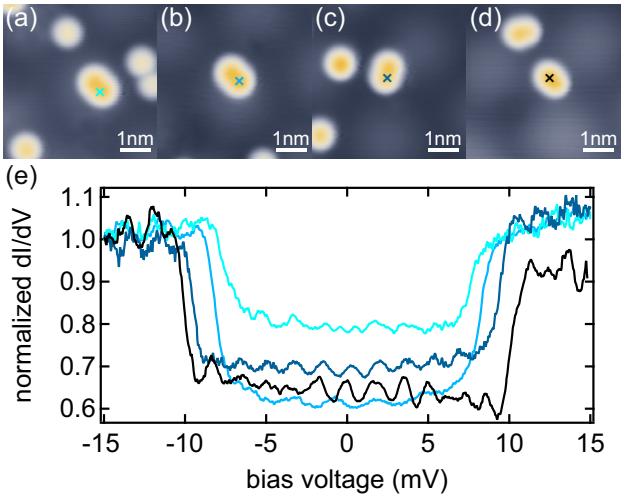

FIG. 3. Antiferromagnetically coupled Mn dimers (oval structures) in different locations relative to the moiré structure. (a)–(d) STM topographies of dimers (a) on the maximum, (b) close to the maximum, (c) further from the maximum, and (d) at the minimum of the moiré structure. (e) dI/dV spectra acquired on the dimers shown in (a)–(d), with colors matched to the crosses in (a)–(d). Topographies recorded at 100 mV, 20 pA, setpoints of the recorded spectra 20 mV, 1 nA (b), 20 mV, 3 nA (a) and 15 mV, 3 nA (c),(d). Spectra are normalized for clarity.

rule, this implies a high-spin configuration with $S = 5/2$ and suggests that spin-orbit coupling is weak, so that the interadatom exchange can be modeled by isotropic Heisenberg exchange, $H_{\mathrm{ex}} = J_D \mathbf{S}_A \cdot \mathbf{S}_B$. Here, $\mathbf{S}_{A,B}$ denotes the spins of adatom A,B.

In the absence of hybridization with the substrate, states with magnitude S_{tot} of the total spin $\mathbf{S}_{\mathrm{tot}} = \mathbf{S}_A + \mathbf{S}_B$ will have direct exchange energy

$$E_{\mathrm{ex}}(S_A, S_B; S_{\mathrm{tot}}) = \frac{J_D}{2}\left[S_{\mathrm{tot}}(S_{\mathrm{tot}}+1) - \sum_{j\in\{A,B\}} S_j(S_j+1)\right]. \tag{1}$$

Evaluating the singlet-triplet splitting for $S_A, S_B = 5/2$, we find

$$\Delta = E_{\mathrm{ex}}\left(\frac{5}{2},\frac{5}{2};1\right) - E_{\mathrm{ex}}\left(\frac{5}{2},\frac{5}{2};0\right) = J_D. \tag{2}$$

This splitting is reduced by the hybridization of the adatom d orbitals with the conduction electrons. In general, the d orbitals hybridize with $2S = 5$ (symmetry-adapted) conduction-electron channels [33]. Since the substrate breaks rotational symmetry, the strength of hybridization V_m depends on the channel m. The energies of the singlet and triplet states are then shifted by virtual excitation processes, in which a d electron hops into the substrate or a substrate electron hops into the d shell. Physically, these processes reduce the effective adatom spin, which results in a smaller direct exchange. A detailed calculation in second-order perturbation theory (see the Supplemental Material for details [30]) gives a renormalized singlet-triplet splitting:

$$\Delta = J_D\left\{1 - \frac{2}{5}\sum_m \nu_0 |V_m|^2 \left[\frac{1}{|\epsilon_d|} + \frac{1}{\epsilon_d + U}\right]\right\}. \tag{3}$$

Here, $-\epsilon_d > 0$ is the energy to remove an electron from the filled d shell and $\epsilon_d + U$ the energy to add an electron. The factor 2 in front of the sum over channels accounts for the fact that both adatoms can be excited. The factor $1/5$ results from angular-momentum coupling.

The singlet-triplet spacing can be directly related to experimentally measurable quantities by noting that the exchange coupling between the conduction electrons and the spin-S adatom is given by [33]

$$J_m = \frac{|V_m|^2}{2S}\left[\frac{1}{|\epsilon_d|} + \frac{1}{\epsilon_d + U}\right], \tag{4}$$

so that we can express the singlet-triplet splitting of the $S = 5/2$ Mn dimer as

$$\Delta = J_D\left\{1 - 2\sum_m \nu_0 J_m\right\}. \tag{5}$$

For weak coupling ($\nu_0 J_m \ll 1$), the relative change in the singlet-triplet spacing between minimum (Δ_{min}) and maximum (Δ_{max}) is approximately equal to $\delta \simeq (\Delta_{\mathrm{min}} - \Delta_{\mathrm{max}})/J_D$. Equation (5) relates this directly to the corresponding change in the sum of the dimensionless exchange couplings $\sum_m \nu_0 J_m$ to the substrate. Since information on the exchange couplings $\nu_0 J_m$ can be extracted from the Kondo data on a single adatom, applying this relation to the data in Fig. 3(e) gives direct information on the number of conduction-electron channels coupled to the adatom spins.

For analyzing the number of participating channels, we first assume that the adatom spin is coupled to a single channel. With this assumption, we can extract the dimensionless adatom-substrate exchange coupling $\nu_0 J$ of the single channel by fitting the Kondo peak of the isolated atoms using a program based on Ref. [27]. Showcasing the variation between extremal positions with respect to the moiré pattern, we extracted a value of $\nu_0 J = 0.049$ for the adatom on the moiré minimum and $\nu_0 J = 0.080$ for an atom on the maximum from fitting the Kondo data in Fig. 1(b). Equation (5) (specified to a single channel) then predicts a relative change δ of the singlet-triplet splitting from minimum to maximum by ≈6%. This is clearly smaller than the experimentally observed variation of $> 25\%$ [Fig. 3(e) and Fig. S8 [30]]. We have extracted $\nu_0 J$ for several dozen isolated atoms in various positions across the moiré structure. In all cases, $\nu_0 J$ decreases with increasing distance from the maxima of the moiré pattern [Fig. 1(d)]. The variations of $\nu_0 J$ for similar distances from the moiré maxima partially derive from the lack of rotational symmetry, so that the distance to the moiré maximum does not uniquely specify the adsorption site. Moreover, the fitting procedure contains some uncertainty, as the strength of tunneling T_0^2 and $\nu_0 J$ both affect the peak height. We first determined T_0^2 from a spectrum of an atom subject to a magnetic field (for which the uncertainty is reduced due to the additional magnetic-field induced structure). We then fitted all spectra with the extracted value of T_0^2. To indicate the error margins of the fits, we reran all fits taking extremal values of T_0^2 consistent with the B-field data with sufficient accuracy. The black dashed line in Fig. 1(d) shows a linear guide to the eye for the best fit results, while the red dashed lines indicate the scalings obtained when using the extremal values of T_0^2. We find that with the assumption of a single channel, only the largest variation in $\nu_0 J$ (upper red dashed line) would explain the variation of the singlet-triplet splitting.

We can also apply Eq. (5), when assuming that all five channels are equally coupled. Since each channel renormalizes independently, the value of $\nu_0 J_m$ for any m is equal to that extracted with the single-channel assumption. (In the

leading-logarithm approximation underlying the Kondo fits, the number of channels enters only as an overall prefactor, which can be absorbed into T_0^2.) With this assumption, Eq. (5) predicts a variation in the singlet-triplet spacing, which is larger by a factor of 5 than in the single-channel case. We then find that the observed variation in the singlet-triplet spacing across the moiré structure [Fig. 3(e) and Fig. S8 [30]] would only be consistent with the opposite extreme case [lower red dashed line in Fig. 1(d)]. Thus, while the uncertainties of the fitting procedure preclude a fully quantitative analysis, our results strongly suggest that the Mn atoms have substantial coupling to several conduction-electron channels in the Au(111) substrate.

In conclusion, we varied the adatom-substrate exchange of Mn monomers and dimers by exploiting the moiré pattern of a MoS_2 layer on Au(111). The moiré structure imprints density-of-states modulations, which in turn affect the Kondo resonance of the monomer and the singlet-triplet splitting of antiferromagnetically coupled dimers. Relating these variations through a theoretical analysis, we find evidence that the adatoms are coupled to multiple conduction-electron channels. This contrasts with the commonly made assumption that adatoms couple only to a single channel of a metallic substrate. Our results show that this assumption is violated in the perturbative limit. For the fully developed Kondo effect, relatively small differences in $\nu_0 J_m$ between channels result in large differences in the associated Kondo temperatures $T_{K,m} \propto e^{-1/\nu_0 J_m}$. Then, the single-channel approximation can still be adequate provided that only the first stage of the resulting multistage Kondo screening is accessible in experiment. Interestingly, coupling to multiple conduction-electron channels has previously been invoked to explain the appearance of multiple Yu-Shiba-Rusinov states induced by magnetic adatoms on superconductors [34,35]. Our results emphasize that adatom dimers realize a rich two-impurity problem. While theoretical studies have focused on spin-1/2 impurities, adatom dimers typically have higher spins and couple to multiple conduction-electron channels.

We acknowledge financial support by the Deutsche Forschungsgemeinschaft (DFG, German Research Foundation) through Projects No. 328545488 (CRC 227, Project No. B05) and No. 277101999 (CRC 183, Project No. C02 and a Mercator professorship), as well as by the National Science Foundation through Grant No. NSF DMR-2002275.

[1] V. Madhavan, W. Chen, T. Jamneala, M. F. Crommie, and N. S. Wingreen, Tunneling into a single magnetic atom: Spectroscopic evidence of the Kondo resonance, Science **280**, 567 (1998).

[2] J. Li, W.-D. Schneider, R. Berndt, and B. Delley, Kondo Scattering Observed at a Single Magnetic Impurity, Phys. Rev. Lett. **80**, 2893 (1998).

[3] Y.-H. Zhang, S. Kahle, T. Herden, C. Stroh, M. Mayor, U. Schlickum, M. Ternes, P. Wahl, and K. Kern, Temperature and magnetic field dependence of a Kondo system in the weak coupling regime, Nat. Commun. **4**, 2110 (2013).

[4] A. J. Heinrich, J. A. Gupta, C. P. Lutz, and D. M. Eigler, Single-atom spin-flip spectroscopy, Science **306**, 466 (2004).

[5] M. A. Ruderman and C. Kittel, Indirect exchange coupling of nuclear magnetic moments by conduction electrons, Phys. Rev. **96**, 99 (1954).

[6] T. Kasuya, A theory of metallic ferro- and antiferromagnetism on Zener's model, Prog. Theor. Phys. **16**, 45 (1956).

[7] K. Yosida, Magnetic properties of Cu-Mn alloys, Phys. Rev. **106**, 893 (1957).

[8] I. Dzyaloshinsky, A thermodynamic theory of weak ferromagnetism of antiferromagnetics, J. Phys. Chem. Solids **4**, 241 (1958).

[9] T. Moriya, Anisotropic superexchange interaction and weak ferromagnetism, Phys. Rev. **120**, 91 (1960).

[10] P. Wahl, P. Simon, L. Diekhöner, V. S. Stepanyuk, P. Bruno, M. A. Schneider, and K. Kern, Exchange Interaction Between Single Magnetic Adatoms, Phys. Rev. Lett. **98**, 056601 (2007).

[11] F. Meier, L. Zhou, J. Wiebe, and R. Wiesendanger, Revealing magnetic interactions from single-atom magnetization curves, Science **320**, 82 (2008).

[12] A. Khajetoorians, M. Steinbrecher, M. Ternes, M. Bouhassoune, M. dos Santos Dias, S. Lounis, J. Wiebe, and R. Wiesendanger, Tailoring the chiral magnetic interaction between two individual atoms, Nat. Commun. **7**, 10620 (2016).

[13] C. Jayaprakash, H. R. Krishna-murthy, and J. W. Wilkins, Two-Impurity Kondo Problem, Phys. Rev. Lett. **47**, 737 (1981).

[14] B. A. Jones, C. M. Varma, and J. W. Wilkins, Low-Temperature Properties of the Two-Impurity Kondo Hamiltonian, Phys. Rev. Lett. **61**, 125 (1988).

[15] N. Tsukahara, S. Shiraki, S. Itou, N. Ohta, N. Takagi, and M. Kawai, Evolution of Kondo Resonance from a Single Impurity Molecule to the Two-Dimensional Lattice, Phys. Rev. Lett. **106**, 187201 (2011).

[16] H. Prüser, P. E. Dargel, M. Bouhassoune, R. G. Ulbrich, T. Pruschke, S. Lounis, and M. Wenderoth, Interplay between the Kondo effect and the Ruderman–Kittel–Kasuya–Yosida interaction, Nat. Commun. **5**, 5417 (2014).

[17] A. Spinelli, M. Gerrits, R. Toskovic, B. Bryant, M. Ternes, and A. F. Otte, Exploring the phase diagram of the two-impurity Kondo problem, Nat. Commun. **6**, 10046 (2015).

[18] M. Moro Lagares, R. Korytar, M. Piantek, R. Robles, N. Lorente, J. Pascual, M. Ibarra, and D. Serrate, Real space manifestations of coherent screening in atomic scale Kondo lattices, Nat. Commun. **10**, 2211 (2019).

[19] A. A. Khajetoorians, D. Wegner, A. F. Otte, and I. Swart, Creating designer quantum states of matter atom-by-atom, Nat. Rev. Phys. **1**, 703 (2019).

[20] J. C. Oberg, M. R. Calvo, F. Delgado, M. Moro-Lagares, D. Serrate, J. Fernandez-Rossier, and C. F. Hirjibehedin,

Control of single-spin magnetic anisotropy by exchange coupling, Nat. Nanotechnol. **9**, 64 (2014).

[21] J. Ren, H. Guo, J. Pan, Y. Y. Zhang, X. Wu, H.-G. Luo, S. Du, S. T. Pantelides, and H.-J. Gao, Kondo effect of cobalt adatoms on a graphene monolayer controlled by substrate-induced ripples, Nano Lett. **14**, 4011 (2014).

[22] P. Jacobson, T. Herden, M. Muenks, G. Laskin, O. Brovko, V. Stepanyuk, M. Ternes, and K. Kern, Quantum engineering of spin and anisotropy in magnetic molecular junctions, Nat. Commun. **6**, 8536 (2015).

[23] S. Trishin, C. Lotze, N. Bogdanoff, F. von Oppen, and K. J. Franke, Moiré Tuning of Spin Excitations: Individual Fe Atoms on $MoS_2/Au(111)$, Phys. Rev. Lett. **127**, 236801 (2021).

[24] S. S. Grønborg, S. Ulstrup, M. Bianchi, M. Dendzik, C. E. Sanders, J. V. Lauritsen, P. Hofmann, and J. A. Miwa, Synthesis of epitaxial single-layer MoS_2 on $Au(111)$, Langmuir **31**, 9700 (2015).

[25] N. Krane, C. Lotze, and K. J. Franke, Moiré structure of MoS_2 on Au(111): Local structural and electronic properties, Surf. Sci. **678**, 136 (2018).

[26] H. Bana, E. Travaglia, L. Bignardi, P. Lacovig, C. E. Sanders, M. Dendzik, M. Michiardi, M. Bianchi, D. Lizzit, F. Presel, D. D. Angelis, N. Apostol, P. K. Das, J. Fujii, I. Vobornik, R. Larciprete, A. Baraldi, P. Hofmann, and S. Lizzit, Epitaxial growth of single-orientation high-quality MoS_2 monolayers, 2D Mater. **5**, 035012 (2018).

[27] M. Ternes, Spin excitations and correlations in scanning tunneling spectroscopy, New J. Phys. **17**, 063016 (2015).

[28] Y. Wang, B. Wang, R. Huang, B. Gao, F. Kong, and Q. Zhang, First-principles study of transition-metal atoms adsorption on MoS_2 monolayer, Physica (Amsterdam) **63E**, 276 (2014).

[29] X. Chen, L. Zhong, X. Li, and J. Qi, Valley splitting in the transition-metal dichalcogenide monolayer via atom adsorption, Nanoscale **9**, 2188 (2017).

[30] See Supplemental Material at http://link.aps.org/supplemental/10.1103/PhysRevLett.130.176201 for theoretical considerations and additional experimental data.

[31] C. F. Hirjibehedin, C. P. Lutz, and A. J. Heinrich, Spin coupling in engineered atomic structures, Science **312**, 1021 (2006).

[32] Y. Mokrousov, G. Bihlmayer, S. Blügel, and S. Heinze, Magnetic order and exchange interactions in monoatomic 3*d* transition-metal chains, Phys. Rev. B **75**, 104413 (2007).

[33] J. R. Schrieffer, The Kondo effect – The link between magnetic and nonmagnetic impurities in metals?, J. Appl. Phys. **38**, 1143 (1967).

[34] M. Ruby, Y. Peng, F. von Oppen, B. W. Heinrich, and K. J. Franke, Orbital Picture of Yu-Shiba-Rusinov Multiplets, Phys. Rev. Lett. **117**, 186801 (2016).

[35] D.-J. Choi, C. Rubio-Verdú, J. De Bruijckere, M. M. Ugeda, N. Lorente, and J. I. Pascual, Mapping the orbital structure of impurity bound states in a superconductor, Nat. Commun. **8**, 15175 (2017).